Catalysis Today 171 (2011) 257–265

Contents lists available at ScienceDirect

Catalysis Today

journal homepage: www.elsevier.com/locate/cattod

Rh-catalyzed syngas conversion to ethanol: Studies on the promoting effect of FeO_x

Jingjuan Wang, Qinghong Zhang, Ye Wang*

State Key Laboratory of Physical Chemistry of Solid Surfaces, National Engineering Laboratory for Green Chemical Productions of Alcohols, Ethers and Esters, College of Chemistry and Chemical Engineering, Xiamen University, Xiamen 361005, China

ARTICLE INFO

Article history:
Received 30 October 2010
Received in revised form 19 February 2011
Accepted 9 March 2011
Available online 8 April 2011

Keywords:
Syngas conversion
Ethanol
Rhodium
Iron oxide
Promoting effect

ABSTRACT

Rhodium catalysts loaded on silica modified by various transition metal oxides were investigated for the conversion of syngas to ethanol. Iron oxide was found to be an efficient promoter for ethanol formation. The increase in iron content up to 5 wt% significantly increased CO conversion and ethanol selectivity. The preparation method used for introducing FeO_x was found to affect both the conversion and the selectivity significantly. The catalyst prepared by the impregnation of a FeO_x–SiO_2 composite, which was synthesized by a sol–gel technique preliminarily, with $Rh(NO_3)_3$ aqueous solution provided better ethanol formation activity than those prepared by co-impregnation and co-sol–gel methods. An ethanol selectivity of 42% was achieved at CO conversion of 12% over a 5 wt% Rh/(5 wt% FeO_x–SiO_2) catalyst prepared by this method. Larger interfaces between Rh and FeO_x species were proposed to be a crucial factor for obtaining higher ethanol selectivity. The co-existence of Rh^{3+} with Rh^0 and the size of Rh particles also played key roles in ethanol formation.

1. Introduction

Catalytic transformations of syngas (H_2 + CO), which can be produced from non-petroleum carbon resources including natural gas, coal, and biomass, into clean fuels and valuable chemicals have attracted much attention in recent years because of the global demand for the decrease in the dependence on petroleum [1,2]. Ethanol is one of the attractive target products in syngas transformations, because it can be used as a fuel or fuel additive and a potential source of hydrogen for fuel cells, and it can also serve as a feedstock for the production of a variety of chemicals and polymers [3,4]. Many catalysts, particularly Rh-, Co-, Cu- and Mo-based catalysts, have been reported to be capable of catalyzing the conversion of syngas to ethanol [3,4]. However, these catalysts still suffer from lower productivity. Relatively high ethanol selectivity (40–50%) can only be achieved at low CO conversions (typically <10%). It is worthy mentioning that Tsubaki and co-workers [5,6] have developed an intriguing method for ethanol synthesis from dimethyl ether and syngas using the combined zeolite (e.g., H-ZSM-5) and metal (e.g., Cu/ZnO) catalysts.

Among the catalysts reported to date for the direct conversion of syngas to ethanol, supported Rh shows the most promising ethanol formation activity [3,4,7–14]. However, the main products over the supported single Rh catalysts are typically hydrocarbons (particularly methane) [3,4]. The presence of a promoter (e.g., transition metal oxide such as MnO_x, VO_x, or FeO_x) or the combination of several promoters is required for obtaining higher ethanol selectivity [7–14]. The understanding of the functioning mechanism of the promoter will certainly be helpful for the rational design of efficient catalysts for ethanol synthesis. A few studies have demonstrated that the location of promoter (or the contact between promoter and Rh) is quite important for obtaining better catalytic performances [8,15,16]. Thus far, many of the reported studies have employed co-impregnation or sequential impregnation for introducing the transition metal promoters [7–14]. However, these methods cannot ensure the high dispersion of promoters on support and the contact between Rh and transition metal oxide promoters.

The sol–gel technique is known to be capable of producing catalysts with homogeneously distributed supported species [17]. Recently, we prepared transition metal oxide-containing SiO_2 composites using the sol–gel technique and investigated the catalytic performances of Rh catalysts supported on these composite oxides with highly dispersed transition metal oxide promoters for syngas conversions. Herein, we report the catalytic behaviors and the structural features of these catalysts with finely dispersed promoters. The effect of catalyst preparation methods is also discussed to gain insights into the active sites.

---

* Corresponding author. Tel.: +86 592 2186156; fax: +86 592 2183047.
E-mail address: wangye@xmu.edu.cn (Y. Wang).

0920-5861/$ – see front matter © 2011 Elsevier B.V. All rights reserved.
doi:10.1016/j.cattod.2011.03.023

2. Experimental

2.1. Catalyst preparation

Transition metal oxide (MO_x)–SiO_2 composites (denoted as MO_x–SiO_2 hereafter) were prepared by the sol–gel technique [17]. Typically, tetraethyl orthosilicate (TEOS) and the precursor of transition metal oxide (metal nitrates except for NH_4VO_3 used for VO_x-modified SiO_2) were dissolved in the mixture of water and ethylene glycol, and a homogeneous sol was obtained. The sol was then heated at 343 K for 16 h to form a homogenous gel. After being dried at 383 K in air for 12 h, the gel was calcined at 623 K for 6 h in air. The supported Rh catalysts were prepared by incipient wetness impregnation method using $Rh(NO_3)_3$ as the precursor of Rh. After being dried at 383 K for 12 h in air, the supported catalyst was calcined at 623 K in air for 6 h and finally reduced by H_2 at 573 K for 2 h. The catalyst prepared by this procedure was denoted as Rh/(MO_x–SiO_2).

Co-impregnation and co-sol–gel methods were also employed for the preparation of FeO_x-promoted Rh catalysts supported on SiO_2. For the co-impregnation method, the powdery SiO_2, which was prepared preliminarily by the sol–gel technique described above, was added into the mixed aqueous solution containing $Rh(NO_3)_3$ and $Fe(NO_3)_3$, followed by drying at 383 K for 12 h, calcination at 623 K for 6 h, and H_2 reduction at 573 K for 2 h. For the co-sol–gel method, TEOS, $Rh(NO_3)_3$, and $Fe(NO_3)_3$ were dissolved in the mixture of water and ethylene glycol, and the mixture underwent heating at 343 K to form a homogenous gel. After being dried at 383 K in air for 12 h, the sample was calcined at 623 K for 6 h in air, followed by H_2 reduction at 573 K for 2 h. The catalysts prepared by the co-impregnation and co-sol–gel methods were denoted as (Rh–FeO_x)/SiO_2 and Rh–FeO_x–SiO_2, respectively.

2.2. Catalytic reaction

Catalytic reactions were performed on a fixed-bed reactor operated at 2 MPa. The catalyst loaded in the reactor was pretreated by H_2 at 573 K for 2 h. After the catalyst was cooled down to the reaction temperature (typically 523 K), the syngas with a H_2/CO ratio of 2.0 was introduced into the reactor. Typical reaction conditions were as follows: pressure (P) = 2 MPa, H_2/CO = 2, temperature (T) = 523 K, WHSV = 8000 mL g(cat)$^{-1}$ h^{-1}. The products were analyzed by on-line gas chromatography.

2.3. Catalyst characterization

XRD patterns were collected on a Philips X'Pert Pro Super X-ray diffractometer equipped with X'Celerator and Xe detection systems. Cu K_α radiation (40 kV and 30 mA) was used as the X-ray source. X-ray photoelectron spectra (XPS) were recorded with a Quantum 2000 Scanning ESCA Microprob instrument (Physical Electronics) using Al–K_α radiation. The binding energy was calibrated using C_{1s} photoelectron peak at 284.6 eV as a reference. Transmission electron microscopy (TEM) measurements were performed on a JEM-2100 electron microscope operated at an acceleration voltage of 200 kV. The mean sizes of Rh particles were estimated from TEM micrographs by counting ca. 150–200 particles.

H_2 temperature-programmed reduction (H_2-TPR) was performed using a Micromeritics AutoChem 2920 II instrument. Typically, after the pretreatment of sample loaded in a quartz reactor and cooling to 303 K, a H_2–Ar gas mixture was introduced into the reactor, and the temperature was raised to 1073 K at a rate of 10 K min^{-1}. H_2 consumption was monitored by a thermal conductivity detector. CO chemisorption was carried out with a Micromeritics ASAP 2010 C. After the sample was pretreated by H_2 reduction at 573 K and evacuation, CO chemisorption was performed at 308 K. After the first isotherm (total CO uptake), the sample was evacuated for 10 min, and the second isotherm (reversible CO uptake) was measured. The amount of the chemisorbed CO (irreversible CO uptake) was calculated using the difference between the total and reversible CO uptakes.

3. Results and discussion

3.1. Catalytic behaviors of promoted Rh catalysts supported on SiO_2

3.1.1. Catalytic performances of Rh catalysts loaded on various MO_x–SiO_2 composites

Table 1 shows the catalytic performances of Rh catalysts loaded on various MO_x–SiO_2 (M = transition metal) composites prepared by the sol–gel method. Under our reaction conditions, the 1.0 wt% Rh/SiO_2 exhibited a CO conversion of 0.7% and a CH_4 selectivity of 59%. The selectivities of C_2H_5OH and CH_3OH over this catalyst were 9.5% and 4.9%, respectively. The presence of a transition metal oxide (MO_x) modifier listed in Table 1 increased the conversion of CO and decreased the selectivity of CH_4, which is a highly undesirable by-product. A CO conversion of 93% was obtained over the Rh/(CoO_x–SiO_2) catalyst, and this catalyst showed higher selectivities to CO_2 and C_2^+ hydrocarbons. We speculate that the outstandingly high activity of this catalyst is due to the catalytic functions of cobalt, since cobalt is a well-known active catalyst in Fischer–Tropsch (FT) synthesis for the production of linear long-chain hydrocarbons [1,2]. However, this catalyst only provided a quite low selectivity to C_2H_5OH (1.8%). On the other hand, the catalyst containing MnO_x, CrO_x, FeO_x, or VO_x promoter exhibited relatively higher C_2H_5OH selectivity (≥20%). The selectivity of CH_4 became significantly lower over the Rh/(MnO_x–SiO_2) and Rh/(FeO_x–SiO_2) catalysts. Among the catalysts showing C_2H_5OH

Table 1
Catalytic performances of Rh catalysts loaded on various transition metal oxide-modified SiO_2.[a]

Catalysts[b]	CO conv. (%)	Selectivity (%)					EtOH yield (%)
		CO_2	CH_4	$C2^+$ HC[c]	MeOH	EtOH	
Rh/SiO_2	0.7	0	59	7.1	4.9	9.5	0.1
Rh/(VO_x–SiO_2)	5.0	0	45	20	3.7	20	1.0
Rh/(CrO_x–SiO_2)	3.0	0	38	5.1	28	22	0.7
Rh/(MnO_x–SiO_2)	1.5	4.1	15	6.0	17	39	0.6
Rh/(FeO_x–SiO_2)	6.3	3.8	21	12	33	21	1.3
Rh/(CoO_x–SiO_2)	93	21	46	27	1.9	1.8	1.6
Rh/(ZrO_x–SiO_2)	4.9	1.3	44	17	15	19	0.9
Rh/(MoO_x–SiO_2)	7.1	4.3	49	22	14	5.6	0.4

[a] Reaction conditions: H_2/CO = 2; WHSV = 8000 mL g(cat)$^{-1}$ h^{-1}; P = 2.0 MPa; T = 523 K.

[b] The loading of Rh was 1.0 wt%; the content of MO_x was 10 wt%.

[c] C_2^+ hydrocarbons.

Table 2
Catalytic performances of Rh catalysts loaded on FeO_x–SiO_2 with different Fe contents.[a]

Fe content (wt%)	CO conv. (%)	Selectivity (%)					EtOH yield (%)
		CO_2	CH_4	C_2^+ HC[b]	MeOH	EtOH	
0	0.7	0	59	7.1	4.9	9.5	0.1
1.0	2.7	3.7	30	4.5	23	31	0.8
2.0	3.5	2.3	29	3.0	22	32	1.1
5.0	5.3	2.3	25	5.8	25	37	2.0
10	6.3	3.8	21	12	33	21	1.3
20	8.2	4.2	18	13	35	19	1.6

[a] Reaction conditions: $H_2/CO = 2$; WHSV = 8000 mL g(cat)$^{-1}$ h^{-1}; $P = 2.0$ MPa; $T = 523$ K. Rh loading, 1.0 wt%. The Fe content was calculated on the basis of Fe_2O_3.
[b] C_2^+ hydrocarbons.

Table 3
Catalytic performances of Rh catalysts loaded on FeO_x–SiO_2 with different Rh loadings.[a]

Rh loading (wt%)	CO conv. (%)	Selectivity (%)					EtOH yield (%)
		CO_2	CH_4	C_2^+ HC[b]	MeOH	EtOH	
0	Trace	–	–	–	–	–	–
1.0	5.3	2.3	25	5.8	25	37	2.0
2.0	7.6	2.3	24	7.5	20	37	2.8
4.0	9.5	3.0	23	3.9	21	44	4.2
5.0	12.4	3.5	26	5.2	18	42	5.2

[a] Reaction conditions: $H_2/CO = 2$; WHSV = 8000 mL g(cat)$^{-1}$ h^{-1}; $P = 2.0$ MPa; $T = 523$ K. Fe content, 5.0 wt%.
[b] C_2^+ hydrocarbons.

selectivities ≥20%, the Rh/(FeO_x–SiO_2) catalyst provided the highest CO conversion. Therefore, considering the balance of CO conversion and C_2H_5OH selectivity, we selected the Rh/(FeO_x–SiO_2) catalyst for further studies.

3.1.2. Catalytic performances of Rh catalysts loaded on FeO_x–SiO_2

We have examined the effect of Fe content in the Rh/(FeO_x–SiO_2) catalysts on their catalytic performances, and the results are shown in Table 2. The loading of Rh was fixed at 1.0 wt%. The increase in Fe content significantly increased the conversion of CO. The presence of FeO_x led to the formation of CO_2, but the selectivity of CO_2 kept at <5% with Fe contents ranging from 0 to 20 wt%. The selectivity of CH_4 decreased monotonically with increasing Fe content. On the other hand, the selectivities to CH_3OH and C_2H_5OH increased significantly after the addition of FeO_x into SiO_2. The selectivity of CH_3OH increased from 4.9% to 35% as the Fe content rose from 0 to 20 wt%, while that of C_2H_5OH reached a maximum (37%) at a Fe content of 5.0 wt%. In other words, the catalyst with an appropriate content of Fe is required for obtaining the highest C_2H_5OH formation activity.

We further investigated the effect of Rh loadings on catalytic behaviors of the Rh/(FeO_x–SiO_2) catalysts with a Fe content of 5.0 wt%. As shown in Table 3, with increasing Rh loadings, CO conversion increased remarkably, but the product selectivity did not undergo significant changes at the same time. Over the 2 wt% Rh/(5 wt% FeO_x–SiO_2) catalyst, the conversion of CO and the selectivity of C_2H_5OH were 7.6% and 37%, respectively. Such a C_2H_5OH selectivity was better than those reported over VO_x-, LaO_x-, FeO_x-, and MnO_x-promoted Rh/SiO_2 catalysts prepared by co-impregnation or sequential impregnation methods [12,13], and was similar to that reported over a 2% Rh–5% Fe/TiO_2 catalyst [10,16]. The increase in Rh loadings to 4 wt% or 5 wt% in our case further raised C_2H_5OH selectivity, and a 42% C_2H_5OH selectivity was achieved at 12.4% CO conversion over our 5 wt% Rh/(5 wt% FeO_x–SiO_2) catalyst. To the best of our knowledge, this is one of the best combinations of CO conversion and C_2H_5OH selectivity reported to date.

We have also investigated the effect of temperature of H_2 reduction for the 1.0 wt% Rh/(5.0 wt% FeO_x–SiO_2) catalyst on catalytic performances, and the results are shown in Table 4. This series of catalysts were calcined at 573 K before reduction. Without H_2 pre-reduction, CO conversion and C_2H_5OH selectivity were 5.0% and 26%, respectively. In this case, the catalyst could still be reduced in situ in the reactant gas (H_2 + CO) flow. The pre-reduction of catalyst by H_2 at 373–573 K enhanced both CO conversion and C_2H_5OH selectivity. However, higher reduction temperatures (≥673 K) decreased CO conversion and C_2H_5OH selectivity. Thus, a proper reduction temperature is also crucial for obtaining better C_2H_5OH selectivities and higher CO conversions.

3.1.3. Catalytic performances of FeO_x-promoted Rh catalysts prepared by different methods

Table 5 shows the catalytic behaviors of FeO_x-promoted Rh catalysts prepared by different methods. The catalytic performance

Table 4
Catalytic performances of the 1.0 wt% Rh/(5.0 wt% FeO_x–SiO_2) catalysts pre-reduced at different temperatures.[a]

Reduction temp.[b] (K)	CO conv. (%)	Selectivity (%)					EtOH yield (%)
		CO_2	CH_4	C_2^+ HC[c]	MeOH	EtOH	
Without pre-reduction	5.0	3.8	22	8.9	31	26	1.3
373	6.1	2.7	21	4.8	21	45	2.7
473	6.5	2.0	22	4.8	23	41	2.7
573	6.0	2.1	16	3.3	29	42	2.5
673	3.2	2.7	25	7.6	23	38	1.2
773	3.0	2.4	24	6.5	31	31	0.9

[a] Reaction conditions: $H_2/CO = 2/1$; WHSV = 8000 mL g(cat)$^{-1}$ h^{-1}; $P = 2.0$ MPa; $T = 523$ K.
[b] The catalyst was calcined at 573 K before reduction.
[c] C_2^+ hydrocarbons.

Table 5
Catalytic performances of FeO_x-promoted Rh/SiO_2 catalysts prepared by different methods.[a]

Catalysts[b]	CO conv. (%)	Selectivity (%)					EtOH yield (%)
		CO_2	CH_4	C_2^+ HC[c]	MeOH	EtOH	
Rh/SiO_2	0.7	0	59	7.1	4.9	9.5	0.1
$Rh/(FeO_x–SiO_2)$	5.3	2.3	25	5.8	25	37	2.0
$(Rh–FeO_x)/SiO_2$	3.3	0.2	28	5.0	31	26	0.8
$Rh–FeO_x–SiO_2$	2.2	0	28	5.4	31	27	0.6

[a] Reaction conditions: $H_2/CO = 2/1$; WHSV = 8000 mL g(cat)$^{-1}$ h^{-1}; $P = 2.0$ MPa; $T = 523$ K.
[b] The loading of Rh was 1.0 wt%; the content of Fe was 5.0 wt%.
[c] C_2^+ hydrocarbons.

of Rh/SiO_2 without FeO_x modification is also listed in Table 5 for comparison. In each case, the presence of FeO_x could significantly increase CO conversion and C_2H_5OH selectivity. However, the catalytic performance also depended strongly on the preparation method. The catalyst prepared by the impregnation of the $FeO_x–SiO_2$ composite, which was prepared by the sol–gel technique preliminarily, with $Rh(NO_3)_3$ aqueous solution followed by drying, calcination, and H_2 reduction, afforded the highest CO conversion and the best C_2H_5OH selectivity. The catalysts prepared by the co-impregnation [$(Rh–FeO_x)/SiO_2$] and co-sol-gel ($Rh–FeO_x–SiO_2$) methods exhibited significantly lower CO conversions and lower C_2H_5OH selectivities.

3.2. Structural features of FeO_x-promoted Rh catalysts supported on SiO_2

3.2.1. XRD

In the XRD patterns for the 1.0 wt% $Rh/(FeO_x–SiO_2)$ catalysts with different Fe contents (0–20 wt%) (Fig. 1), a broad peak at 2θ of ~23° attributed to amorphous SiO_2 was clearly observed. A very weak peak at 2θ of ~42°, which was assignable to the (1 1 1) reflection of metallic Rh, could also be discerned for some of these samples. No diffraction lines ascribed to any FeO_x-related phases can be observed even when the content of FeO_x was as high as 20 wt%, suggesting that the high dispersion of FeO_x in SiO_2. This is in agreement with the general consensus that the sol–gel technique leads to highly dispersed supported species [17]. With increasing Rh loadings over the 5 wt% $FeO_x–SiO_2$ composite, the intensity of the weak diffraction peak at 2θ of ~42° ascribed to metallic Rh was not significantly enhanced and the peak was still quite broad (Fig. 2). This indicates that the size of Rh particles has not increased significantly even in the catalysts with higher Rh loadings.

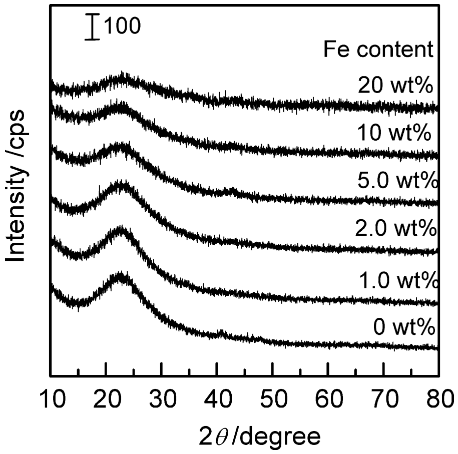

Fig. 1. XRD patterns for 1 wt% Rh/(0–20 wt% $FeO_x–SiO_2$) catalysts with different Fe contents.

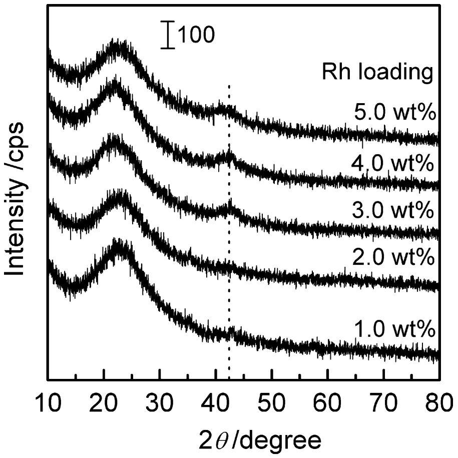

Fig. 2. XRD patterns for (0–5 wt%)Rh/(5 wt% $FeO_x–SiO_2$) catalysts with different Rh loadings.

3.2.2. H_2-TPR

H_2-TPR studies were employed to characterize the reducibility of Rh and Fe species and their interactions in our catalyst without H_2 reduction. The 1.0 wt% Rh/SiO_2 catalyst without FeO_x showed a single peak for the reduction of Rh^{3+} to Rh^0 at 426 K (Fig. 3). The incorporation of FeO_x by each method shifted the reduction peak to higher temperatures, indicating the inhibited reduction of Rh^{3+}. The inhibition of Rh^{3+} reduction in the presence of FeO_x was also reported elsewhere [9,12], and such an inhibition was believed to reflect the interaction between Rh and FeO_x species in the catalyst. Burch and Hayes [9] once argued that the inhibited reduction of Rh^{3+} by the presence of FeO_x could be attributed to

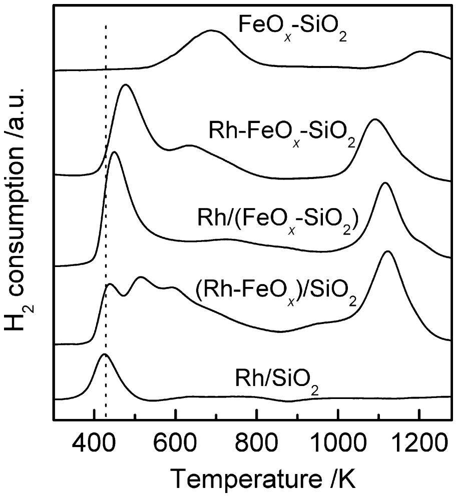

Fig. 3. H_2-TPR profiles for 1 wt% Rh/SiO_2, 5 wt% $FeO_x–SiO_2$, (1 wt% Rh–5 wt% FeO_x)/SiO_2, 1 wt% Rh/(5 wt% $FeO_x–SiO_2$), and 1 wt% Rh–5 wt% $FeO_x–SiO_2$.

covering of Rh species by a layer of FeO_x. The $(Rh–FeO_x)/SiO_2$ catalyst, which was prepared by the co-impregnation method, showed three overlapped reduction peaks in the lower-temperature region (400–800 K) and a reduction peak in the higher-temperature region (>800 K). Our quantitative calculations uncovered that the first peak (439 K) could be ascribed to the reduction of Rh^{3+} to Rh^0, whereas the other two lower-temperature peaks at 515 K and 593 K might be assignable to the reductions of Fe^{3+} into Fe^{2+} and Fe^{2+} partially into Fe^0. The higher-temperature reduction peak at 1123 K for this sample might be assigned to the reduction of the remaining Fe^{2+} to Fe^0 or the reduction of Fe^{3+} possessing strong interactions with the SiO_2 matrix [18–20].

On the other hand, the $Rh/(FeO_x–SiO_2)$ catalyst exhibited a single stronger reduction peak at 449 K in the lower-temperature region and a reduction peak at 1113 K in the higher-temperature region. Our quantitative analysis suggests that the peak at 449 K should comprise not only the reduction of Rh^{3+} into Rh^0 but also the partial reduction of Fe^{3+} into Fe^{2+}, while the reduction peak at 1113 K may correspond to the partial reduction of Fe^{2+} to Fe^0 or the reduction of Fe^{3+} possessing strong interactions with the SiO_2 matrix. Fig. 3 also shows the H_2-TPR profile for the $FeO_x–SiO_2$ sample prepared by the sol–gel method. The peak for the reduction of Fe^{3+} into Fe^{2+} in this sample without Rh occurred at 690 K. Thus, Rh species significantly accelerated the reduction of Fe species in this sample. For the $Rh–FeO_x–SiO_2$ catalyst prepared by the co-sol–gel method, two peaks at 478 K and 637 K were observed in lower-temperature region. The quantitative analysis clarified that the first peak comprised the reductions of Rh^{3+} into Rh^0 and Fe^{3+} partially into Fe^{2+}, while the second peak corresponded to the reductions of the remaining Fe^{3+} into Fe^{2+} and also a small part of Fe^{2+} into Fe^0. The reduction of Rh^{3+} into Rh^0 further shifted to higher temperatures in this sample. The observation that the reductions of Rh^{3+} and Fe^{3+} into Rh^0 and Fe^{2+} occurred simultaneous over the $Rh/(FeO_x–SiO_2)$ catalyst indicates the largest contact boundary between Rh and FeO_x species in this catalyst.

We further performed H_2-TPR studies for 1.0 wt% $Rh/(FeO_x–SiO_2)$ catalysts with different Fe contents. As shown in Fig. 4, with increasing Fe content, the intensity of the lower-temperature peak (400–500 K) increased gradually, further confirming that this peak also comprised the reduction of Fe^{3+} species. No higher-temperature peak was observed for the sample with a Fe content of 2.0 wt%. Our quantitative analysis clarified that the lower-temperature peak for this sample comprised the reductions of Rh^{3+} into Rh^0 and Fe^{3+} into Fe^0. We speculate that most of the FeO_x species are in intimate contact with Rh particles in this sample. The higher-temperature peak was observed for the samples with Fe contents ≥5.0 wt%, and this peak mainly corresponded to the partial reduction of Fe^{2+} into Fe^0 or the reduction of Fe^{3+} possessing strong interaction with SiO_2 matrix. The reductions of Rh^{3+} into Rh^0 and Fe^{3+} into Fe^{2+} occurred mainly at <1000 K. A single reduction peak was observed for this series of catalysts with Fe contents ≤10 wt%. The position of this peak shifted to higher temperatures on increasing Fe content, indicating that the degree of inhibition of Rh^{3+} reduction by FeO_x became larger at higher Fe contents. For the catalyst with a Fe content of 20 wt%, the lower-temperature peak became significantly broader, and a shoulder peak at 728 K appeared. This may imply that some FeO_x species in the catalyst are not in intimate contact with Rh particles.

3.2.3. XPS

XPS studies have been performed to gain information about the chemical state of Rh on catalyst surfaces after reduction at 573 K. Typically, after reduction by H_2 at 573 K, followed by cooling to room temperature in H_2 gas flow, the catalysts were transferred to XPS chamber as soon as possible to avoid the exposure in air for a long time. As shown in Fig. 5, the binding energy of Rh $3d_{5/2}$ over the 1.0 wt% Rh/SiO_2 was 307.2 eV, which could be assigned to that of Rh^0 [21]. Thus, Rh^0 was the dominant Rh species over this catalyst without FeO_x promoter. After the introduction of FeO_x, besides the peak at 307.2–307.4 eV for Rh $3d_{5/2}$, a shoulder peak at 309.3 eV, which could be attributed to Rh^{3+} [21], also appeared. This suggests that some oxidized Rh species also co-exist with Rh^0 on the surfaces of the reduced catalysts containing FeO_x. Moreover, the relative intensity of the shoulder peak attributable to oxidized Rh species depended on the preparation method. We have roughly estimated the molar ratio of Rh^{3+}/Rh^0 from XPS, and the results are summarized in Table 6. The ratio of Rh^{3+}/Rh^0 over the $Rh/(FeO_x–SiO_2)$ catalyst, which exhibited the best catalytic performance for C_2H_5OH formation, was higher than that over the $(Rh–FeO_x)/SiO_2$ catalyst prepared by the co-impregnation but lower than that over the $Rh–FeO_x–SiO_2$ catalyst prepared by the co-sol–gel method.

We also performed XPS studies for the 1.0 wt% $Rh/(FeO_x–SiO_2)$ series of catalysts with different Fe contents. As shown in Fig. 6, the ratio of Rh^{3+}/Rh^0 depended on Fe contents in these samples. The ratio of Rh^{3+}/Rh^0 increased with increasing Fe content up to 10 wt%, and a further increase in Fe content did not significantly alter the ratio of Rh^{3+}/Rh^0. XPS studies for the 1.0 wt%

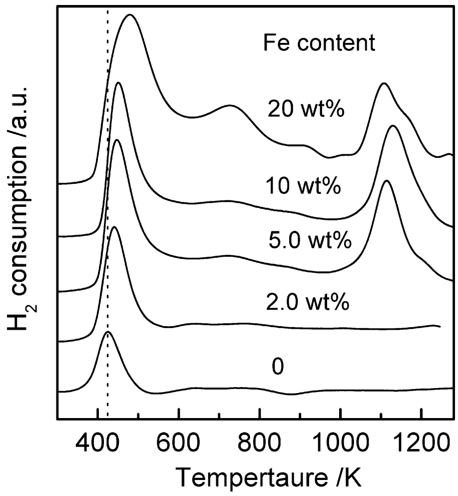

Fig. 4. H_2-TPR profiles for 1 wt% $Rh/(FeO_x–SiO_2)$ samples with different Fe contents.

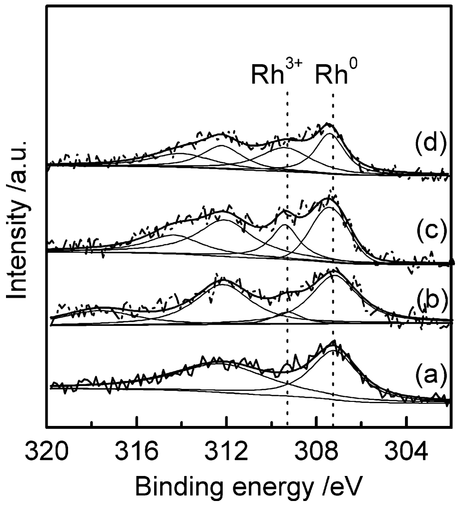

Fig. 5. XPS spectra. (a) 1 wt% Rh/SiO_2, (b) (1 wt% Rh–5 wt% FeO_x)/SiO_2, (c) 1 wt% Rh/(5 wt% $FeO_x–SiO_2$), (d) 1 wt% Rh–5 wt% $FeO_x–SiO_2$.

Table 6
The reducibility, metal dispersion and particles size of Rh/SiO_2 and Fe-modified Rh-based samples prepared by different methods.

Catalyst[a]	Rh^{3+}/Rh^{0}[b]	Rh size[c]	Rh dispersion[d]	Chemisorbed CO/Rh
Rh/SiO_2	~0	2.8	0.27	0.28
Rh/(5 wt% FeO_x–SiO_2)	0.75	3.4	0.22	0.14
(Rh–5 wt% FeO_x)/SiO_2	0.25	6.5	0.12	0.070
Rh–5 wt% FeO_x–SiO_2	1.1	5.0	0.15	0.048
Rh/(2 wt% FeO_x–SiO_2)	0.57	2.6	0.29	0.26
Rh/(10 wt% FeO_x–SiO_2)	1.1	4.5	0.17	0.07
Rh/(20 wt% FeO_x–SiO_2)	1.1	4.8	0.16	0.02
Rh/(5 wt% FeO_x–SiO_2)[e]	1.1	2.2	0.34	0.40
Rh/(5 wt% FeO_x–SiO_2)[f]	0.72	–	–	0.29
Rh/(5 wt% FeO_x–SiO_2)[g]	0.23	11	0.068	0.060
Rh/(5 wt% FeO_x–SiO_2)[h]	0.11	–	–	0.03

[a] Rh loading was 1.0 wt%.
[b] Estimated from XPS spectra
[c] Evaluated from TEM measurements.
[d] Estimated by the following relationship, Rh dispersion = 0.75/[Rh size/nm] [22].
[e] Reduced at 373 K (the standard reduction temperature was 573 K).
[f] Reduced at 474 K (the standard reduction temperature was 573 K).
[g] Reduced at 673 K (the standard reduction temperature was 573 K).
[h] Reduced at 773 K (the standard reduction temperature was 573 K).

Rh/(5.0 wt% FeO_x–SiO_2) catalysts reduced at different temperatures (373–773 K) further uncovered that a higher reduction temperature resulted in a lower Rh^{3+}/Rh^{0} ratio (Table 6).

3.2.4. *TEM and CO chemisorption*

The size and dispersion of Rh particles are also expected to influence the catalytic performances. Thus, we have carried out TEM and CO chemisorption measurements for some of our catalysts. Fig. 7 shows the TEM micrographs and the corresponding Rh particle size distributions for the 5.0 wt% FeO_x-promoted 1.0 wt% Rh catalysts prepared by different methods. Without FeO_x, the mean size of Rh particles (d) over the 1.0 wt% Rh/SiO_2 sample was 2.8 nm. The mean size of Rh particles in the 1.0 wt% Rh/(FeO_x–SiO_2) catalyst became slightly larger (3.4 nm), whereas the co-impregnation method resulted in the biggest Rh particles (mean size, 6.5 nm). TEM studies for the 1.0 wt% Rh/(FeO_x–SiO_2) catalysts with different Fe contents showed that the mean size of Rh particles increased with Fe content (Table 6). This observation further confirms that the presence of FeO_x slightly increases the size of Rh particles. Fig. 8 shows the TEM images and the corresponding Rh particle size distributions for the 1 wt% Rh/(5 wt% FeO_x–SiO_2) catalysts after H_2 reduction at three different temperatures. The increase in H_2 reduction temperature caused the rise in the mean size of Rh particles. Particularly, when the reduction temperature was raised from 573 K to 673 K, the mean size of Rh particles increased remarkably from 3.4 nm to 10.8 nm.

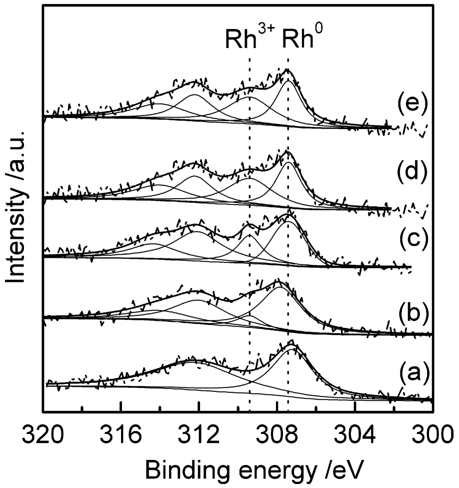

Fig. 6. XPS spectra for 1 wt% Rh/(FeO_x–SiO_2) samples with different Fe contents. Fe contents: (a) 0, (b) 2 wt%, (c) 5 wt%, (d) 10 wt%, (e) 20 wt%.

By assuming the spherical metal particles, Rh dispersion could be estimated by the following relationship, dispersion = 0.75/d (nm) [22]. The value of Rh dispersion thus estimated for each catalyst is listed in Table 6. We have also measured the amount of CO chemisorption, and the molar ratios of chemisorbed CO/Ru for different catalysts are summarized in Table 6. The chemisorbed CO/Rh ratio was almost the same with the Rh dispersion evaluated from the mean size of Rh particles for the Rh/SiO_2 catalyst. However, for most of the FeO_x-promoted catalysts listed in Table 6, the chemisorbed CO/Rh ratios were lower than the Rh dispersions estimated from the mean Rh particle sizes. We speculate that this may be because a fraction of Rh species are in oxidized state (Rh^{3+}), and CO may not be chemisorbed on these Rh^{3+} species. By taking into account the Rh^{3+}/Rh^{0} value evaluated from XPS studies (Table 6), we calculated the corrected Rh dispersion, which only considers the fraction of surface Rh^{0} in the total Rh atoms. The corrected Rh dispersion was similar to the chemisorbed CO/Rh ratio for the Rh/(5 wt% FeO_x–SiO_2) catalyst. However, the chemisorbed CO/Rh ratios were still lower than the corrected Rh dispersions for the (Rh–5 wt% FeO_x)/SiO_2 and the Rh–5 wt% FeO_x–SiO_2 catalysts. It is likely that such lower chemisorbed CO/Rh ratios may arise from the partial covering of the Rh species by FeO_x or SiO_2 in these samples.

3.3. *Discussion on roles of FeO_x promoters*

Our catalytic studies have clarified that, among various transition metal oxides examined (including VO_x, CrO_x, MnO_x, FeO_x, CoO_x, ZrO_x, and MoO_x), FeO_x is the most efficient promoter for SiO_2-supported Rh catalysts for ethanol formation (Table 1). The presence of FeO_x significantly increased CO conversion and ethanol selectivity, whereas CH_4 selectivity was markedly decreased at the same time. There exists an appropriate Fe content for obtaining the maximum ethanol selectivity. A further increase in Fe contents to ≥10 wt% increased methanol selectivity at the sacrifice of ethanol selectivity (Table 2). Furthermore, we have clearly demonstrated that the catalytic performance is strongly dependent on the method of preparing the FeO_x-promoted catalysts. The Rh/(FeO_x–SiO_2) catalyst prepared by the impregnation of the FeO_x–SiO_2 composite, which was synthesized preliminarily by a sol–gel technique, with $Rh(NO_3)_3$ aqueous solution, followed by drying, calcination, and H_2 reduction afforded significantly better catalytic performances for ethanol formation than the (Rh–FeO_x)/SiO_2 and Rh–FeO_x–SiO_2

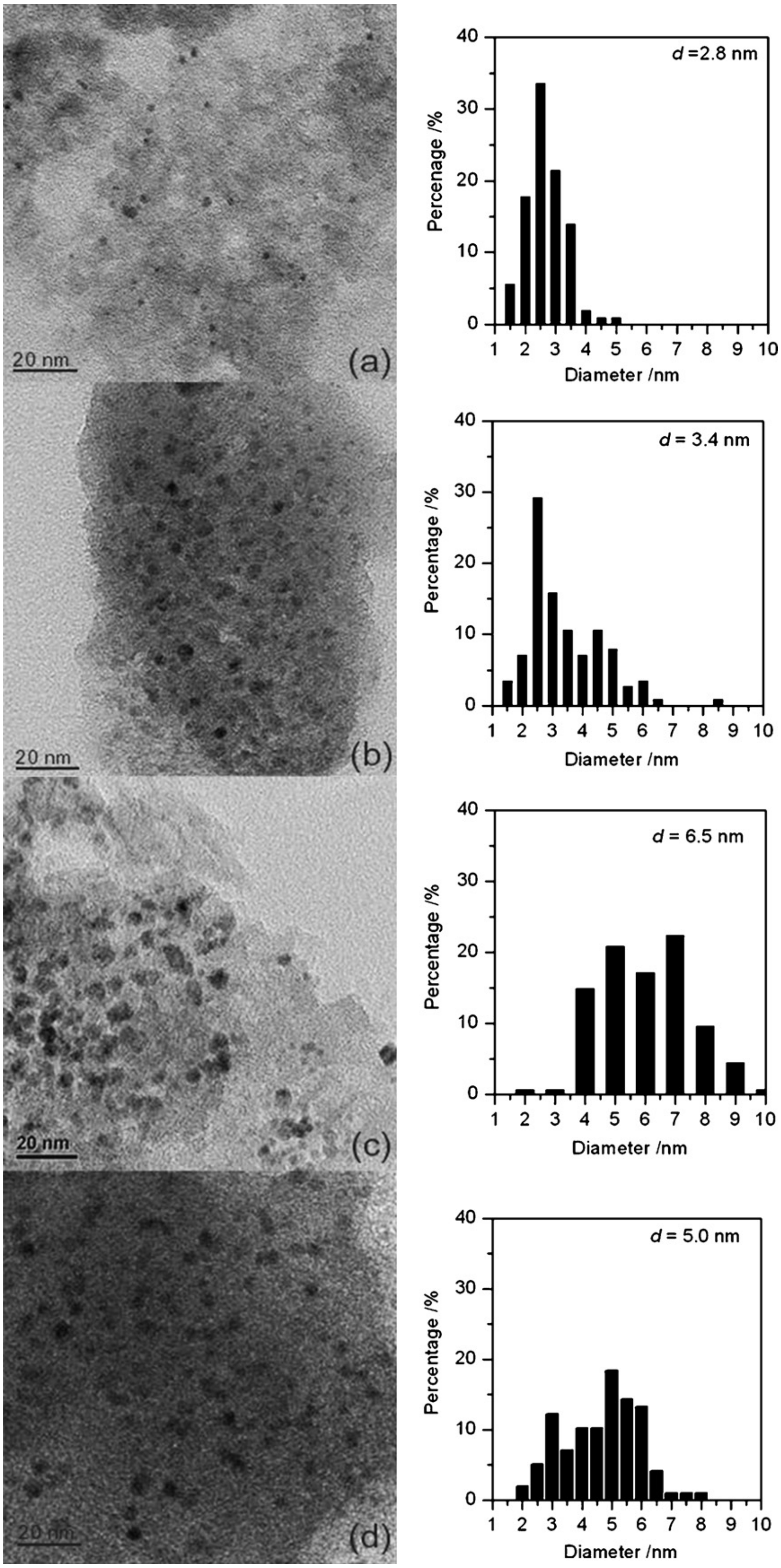

Fig. 7. TEM micrographs and Rh particle size distributions. (a) 1 wt% Rh/SiO_2, (b) 1 wt% Rh/(5 wt% FeO_x–SiO_2), (c) (1 wt% Rh–5 wt% FeO_x)/SiO_2, (d)1 wt% Rh–5 wt% FeO_x–SiO_2.

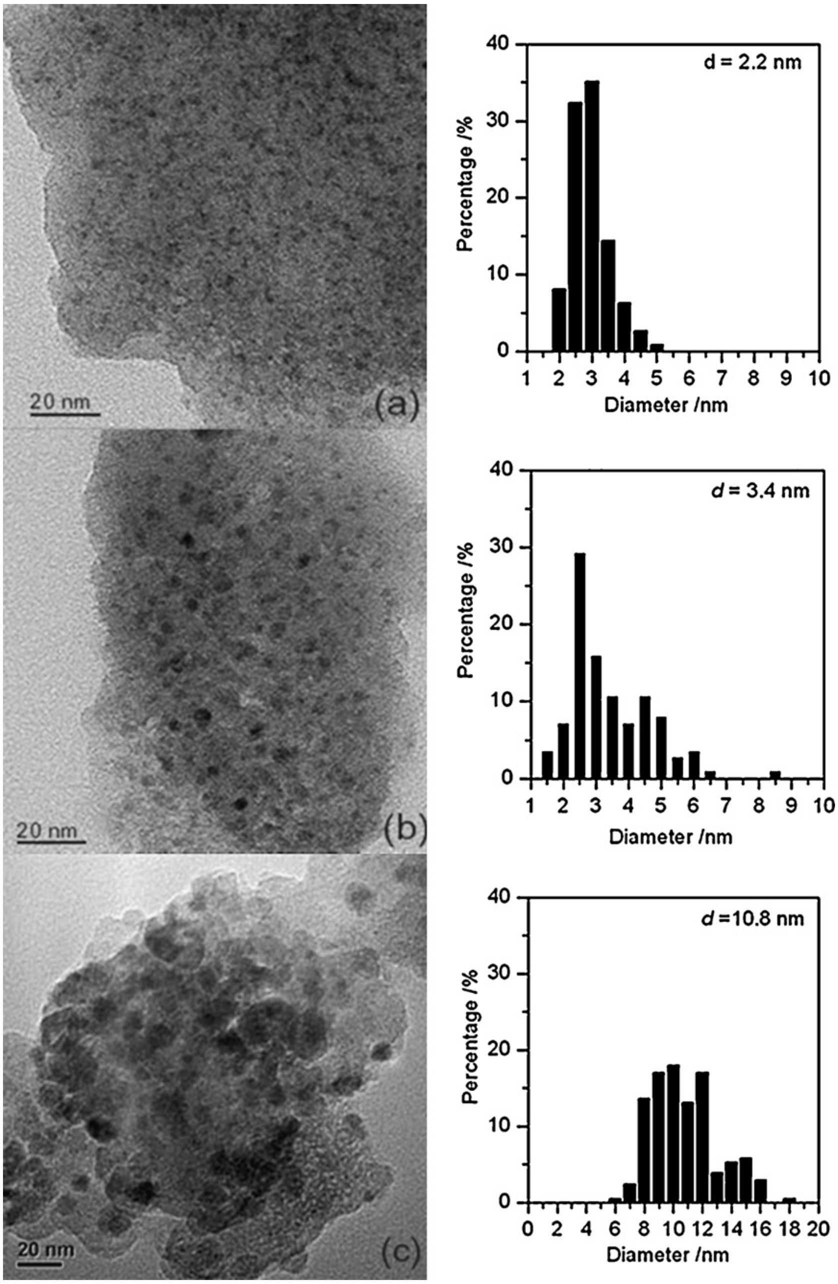

Fig. 8. TEM micrographs and Rh particle size distributions for 1 wt% Rh/(5 wt% FeO_x–SiO_2) samples reduced at different temperatures. Reduction temperatures: (a) 373 K, (b) 573 K, (c) 673 K.

catalysts prepared by co-impregnation and co-sol–gel methods, respectively. The temperature for catalyst reduction has also been found to exert a significant effect on catalytic behaviors.

H_2-TPR studies have clarified that the presence of FeO_x inhibits the reduction of Rh^{3+} into Rh^0 due to the interaction between Rh and Fe species, and the remaining of a part of Rh^{3+} on catalyst surfaces after H_2 reduction has been confirmed by XPS. However, only Rh^0 species was observed over the 1.0 wt% Rh/SiO_2 catalyst without FeO_x promoter. It is established that the selective formation of ethanol requires the balance of CO dissociation, CO insertion, and hydrogenation abilities [3,4,23]. The metallic and oxidized Rh species have been proposed to favor CO dissociation and CO insertion, respectively [23]. We speculate that the co-existence of Rh^{3+} with Rh^0 may increase the CO insertion ability, and thus increase ethanol formation activity. However, a too high ratio of Rh^{3+}/Rh^0 may decrease the CO dissociation ability. This may also lead to the decrease in ethanol selectivity. For example, we observed that the increase in Fe content in the 1.0 wt% Rh/(FeO_x–SiO_2) catalysts to ≥10 wt% resulted in the increase in the ratio of Rh^{3+}/Rh^0 and the decrease in ethanol selectivity. The hydrogenation of non-dissociative CO may give high methanol selectivity over these catalysts (Table 2).

Our H_2-TPR studies also indicated larger interfaces between Rh and FeO_x species in the Rh/(FeO_x–SiO_2) catalyst than in the (Rh–FeO_x)/SiO_2 and Rh–FeO_x–SiO_2 catalysts because the former catalyst showed a single H_2-TPR peak for the simultaneous reductions of Rh^{3+} and Fe^{3+}. Such larger interfaces in the Rh/(FeO_x–SiO_2) catalyst may account for its better catalytic performances (Table 5). Moreover, the catalysts prepared by the co-impregnation and the co-sol–gel methods showed quite lower CO chemisorption amounts (Table 6). Our analysis suggests that this is not only because of the relatively bigger Rh sizes in these samples (Fig. 7) but also probably due to the covering of Rh species by FeO_x or SiO_2. These might result in the lower CO conversion activity for these two catalysts (Table 5).

Higher reduction temperatures ($\geq$673 K) for our 1.0 wt% Rh/(5.0 wt% FeO_x–SiO_2) catalyst caused the formation of larger Rh particles with lower fractions of Rh^{3+}. These catalysts provided lower CO conversions and lower ethanol selectivities (Table 4). The bigger Rh particles may not only decrease the hydrogenation ability but also decrease the interface between Rh and FeO_x species, leading to a lower CO insertion ability. Table 4 shows that these catalysts exhibit relatively higher selectivities to $C_2{}^+$ hydrocarbons. This observation is in agreement with those reported for supported Co and Ru catalysts, where larger metal nanoparticles also favor the chain-growth probability [1,2]. The formation of ethanol is a complex interplay among CO dissociation, CO insertion, and hydrogenation. Our present studies have demonstrated that the interface between Rh and FeO_x species, the Rh^{3+}/Rh^0 ratio, and the size of Rh particles are all important factors determining the catalytic behaviors in the conversion of syngas to ethanol.

4. Conclusions

Rh catalysts supported on transition metal oxide-modified silica were studied for ethanol synthesis from syngas. FeO_x was found to be an efficient promoter for ethanol formation. The presence of FeO_x increased CO conversion and ethanol selectivity, and decreased methane selectivity. An appropriate Fe content was required for obtaining the best catalytic performance. Our characterizations revealed that the presence of FeO_x inhibited the reduction of Rh^{3+}, and a part of Rh^{3+} remained on catalyst surfaces after reduction. The co-existence of metallic and oxidized Rh species may enhance the CO insertion step and increase ethanol formation activity. Our present work clearly demonstrated that the preparation method for introducing FeO_x played a significant role in determining the catalytic performance. The catalyst prepared by the impregnation of the FeO_x–SiO_2 composite, which was synthesized by a sol–gel technique, with $Rh(NO_3)_3$ aqueous solution followed by drying, calcination, and H_2 reduction afforded better ethanol formation activity than those prepared by co-impregnation and co-sol–gel methods. Our characterizations indicated that this catalyst contained larger interfaces between Rh and FeO_x species. The reduction temperature was also found to affect the catalytic performance. Higher reduction temperatures ($\geq$673 K) caused the aggregation of Rh particles, resulting in lower CO conversions and ethanol selectivities. The interfaces between Rh and FeO_x species, the ratio of Rh^{3+}/Rh^0, and the Rh particle size are proposed to be important factors for the selective conversion of syngas to ethanol.

Acknowledgements

This work was supported by the National Natural Science Foundation of China (nos. 20873110, 20923004, and 21033006), the National Basic Program of China (no. 2010CB732303), the Research Fund for the Doctoral Program of Higher Education (no. 20090121110007), and the Key Scientific Project of Fujian Province (no. 2009HZ0002-1).

References

[1] A.Y. Khodakov, W. Chu, P. Fongarland, Chem. Rev. 107 (2007) 1692–1744.
[2] Q. Zhang, J. Kang, Y. Wang, ChemCatChem 2 (2010) 1030–1058.
[3] J.J. Spivey, A. Egbebi, Chem. Soc. Rev. 36 (2007) 1514–1528.
[4] V. Subramani, S.K. Gangwal, Energy Fuels 22 (2008) 814–839.
[5] X. San, Y. Zhang, W. Shen, N. Tsubaki, Energy Fuels 23 (2009) 2843–2844.
[6] X. Li, X. San, Y. Zhang, T. Ichii, M. Meng, Y. Tan, N. Tsubaki, ChemSusChem 3 (2010) 1192–1199.
[7] M.M. Bhasin, W.J. Bartley, P.C. Ellgen, T.P. Wilson, J. Catal. 54 (1978) 120–128.
[8] R. Burch, M.I. Petch, Appl. Catal. A Gen. 88 (1992) 39–60.
[9] R. Burch, M.J. Hayes, J. Catal. 165 (1997) 249–261.
[10] M.A. Haider, M.R. Gogate, R.J. Davis, J. Catal. 261 (2009) 9–16.
[11] J. Gao, X. Mo, A.C. Chien, W. Torres, J.G. Goodwin Jr., J. Catal. 262 (2009) 119–126.
[12] X. Mo, J. Gao, N. Umnajkaseam, J.G. Goodwin Jr., J. Catal. 267 (2009) 167–176.
[13] D. Mei, R. Rousseau, S.M. Kathmann, V.A. Glezakou, M.H. Engelhard, W. Jiang, C. Wang, M.A. Gerber, J.F. White, D.J. Stevens, J. Catal. 271 (2010) 325–342.
[14] N.D. Subramanian, J. Gao, X. Mo, J.G. Goodwin Jr., W. Torres, J.J. Spivey, J. Catal. 272 (2010) 204–209.
[15] M. Ichikawa, T. Fukushima, J. Phys. Chem. 90 (1986) 1222–1224.
[16] M.R. Gogate, R.J. Davis, ChemCatChem 1 (2009) 295–303.
[17] M.V. Landau, in: G. Ertl, H. Knözinger, F. Schüth, J. Weitkamp (Eds.), Handbook of Heterogeneous Catalysis, vol. 1, second ed., Wiley-VCH, Weinheim, 2008, pp. 119–160.
[18] C. Alberto, G. Fajardo, D. Niznansky, Y.N. Guyen, C. Courson, A.C. Roger, Catal. Commun. 9 (2008) 864–869.
[19] T. Kobayashi, N. Guilhaume, J. Miki, N. Kitamura, M. Haruta, Catal. Today 32 (1996) 171–175.
[20] K. Tabata, Y. Takemoto, T. Suzuki, E. Banares, M.A. Pena, J.L.G. Fierro, Catal. Rev. 44 (2002) 1–58.
[21] M. Ojeda, M.L. Granados, S. Rojas, P. Terreros, F.J. García-García, J.L.G. Fierro, Appl. Catal. A Gen. 261 (2004) 47–55.
[22] C.K. Lambert, R.D. Gonzalez, Micropor. Mater. 12 (1997) 179–188.
[23] S.S.C. Chuang, R.W. Stevens Jr., R. Khatri, Top. Catal. 32 (2005) 225–232.